The effect of conducting bounding plates on the onset of Horton-Rogers-Lapwood convection

Abdelkader Mojtabi, D. Andrew Rees

The effect of conducting bounding plates on the onset of Horton–Rogers–Lapwood convection

Abdelkader Mojtabi [a,b,*], D. Andrew S. Rees [c]

[a] Université de Toulouse, INPT, UPS, IMFT (Institut de Mécanique des Fluides de Toulouse), Allée Camille Soula, F-31400 Toulouse, France
[b] CNRS, IMFT, F-31400 Toulouse, France
[c] Department of Mechanical Engineering, University of Bath, Bath BA2 7AY, UK

A B S T R A C T

We present an analytical and numerical stability analysis of the onset of natural convection in a horizontal fluid-saturated porous cavity. The cavity is bounded by thin horizontal plates with uniform thickness whose outer surfaces are subject to a constant heat flux. The main aim is to determine the effect of the presence of the bounding plates on the onset of convection. The onset criterion is found to be sensitively dependent on the relative thickness of the plates and the porous layer, δ, and their relative conductivities, d. For the long wavelength mode it is precisely $Ra_c = 12(1 + \delta d)$.

Keywords:
Convection
Stability
Porous medium

1. Introduction

The knowledge of natural convection in saturated porous media is of considerable interest because of its importance in the modelling of the heat transfer characteristics of geothermal reservoirs and of its numerous fundamental and industrial applications. Reviews of recent developments and publications in this field are given in the books by Nield and Bejan [1], Ingham and Pop [2], Vafaï [3] and most recently by Vadász [4]. The onset of natural convection in horizontal porous media was first studied in the two historic references by Horton and Rogers [5] and Lapwood [6]. This problem was first described as the Horton–Rogers–Lapwood problem by Nield and Bejan [1].

In a porous medium, the use of Darcy's law simplifies considerably the hydrodynamic equations and, in most cases, makes possible an analytical determination of the variation of the critical thermal Rayleigh number Ra_c and wave number k_c, even for the realistic case of impermeable boundaries. Consequently, it has been well known for more than half a century [6] that natural convection in a horizontal porous layer heated from below by a uniform temperature is initiated when the Rayleigh number, based on the permeability of the porous medium, exceeds the value $4\pi^2$. The associated wavenumber in this case is equal to π.

Experimental studies have been undertaken to determine the onset of natural convection in a porous layer bounded by impermeable isothermal planes [7]. The majority of experimental work in this area has been limited to verifying the theoretical predictions. It has also been shown that the presence of lateral boundaries affects the onset of natural convection by restricting the allowable modes [8]. The temperature gradient necessary for convection to start has also been measured [9].

Ribando and Torrance [10] considered a case where a uniform heat flux is applied to the horizontal lower surface and the upper surface is held at a constant temperature, while the vertical walls are adiabatic. This important situation occurs when the layer is heated from below by, say, electric heating elements while the upper surface is maintained at a uniform temperature. They found the critical Rayleigh number and critical wavenumber to be 27.1 and 2.29, respectively. Wang [11] also considered this case and obtained the more accurate value, $Ra_c = 27.096$. Tewari and Torrance [12] followed this with a study of a box with a permeable upper surface and constant temperature lower surface. The number of numerical investigations into two-dimensional large-amplitude convection is also substantial but we refer, in particular, to the work of Riley and Winters [13]; their main aim was to perform a detailed study of bifurcations and modal interactions. They dealt initially with linear stability and, for a cavity of any fixed aspect ratio, showed that an infinitely large set of eigenmodes exists. The preferred mode of convection is the one with the lowest critical Rayleigh number which always has one cell in the vertical direction. The number of cells in the horizontal direction then depends upon the aspect ratio.

* Corresponding author at: Université de Toulouse, INPT, UPS, IMFT (Institut de Mécanique des Fluides de Toulouse), Allée Camille Soula, F-31400 Toulouse, France. Tel.: +33 5 61 55 67 93.
E-mail address: mojtabi@imft.fr (A. Mojtabi).

Nomenclature

A	aspect ratio of the cavity $A = L/H$
a	modified thermal diffusivity of the porous cell $a^* = \lambda^*/(\rho c)_f$
d	thermal conductivity ratio $d = \lambda_s/\lambda_p$
H	height of the porous layer (m)
h	height of the horizontal plates (m)
K	permeability of the porous medium (m^2)
k	wave number
L	length of the cavity (m)
T_1, T_3	temperature inside the lower and upper plates (K)
T_2	temperature inside the porous bulk (K)
Ra	thermal Rayleigh number $Ra = [KHg\beta_T\Delta T]/(\alpha_p \nu)$
Ra_c	critical Rayleigh
$\mathbf{V}$	velocity of the flow ($m\ s^{-1}$)
u, v	velocity components ($m\ s^{-1}$)
t	nondimensional time
q'	uniform heat per unit area ($W\ m^{-2}$)

Greek symbols

α	thermal diffusivity ratio (a_s/a)
β_T	thermal expansion coefficient (K^{-1})
ε^*	porosity of porous medium
ε	normalized porosity
$\theta_{1,3}$	temperature inside lower and upper plates
λ_p	effective thermal conductivity of the porous medium ($W\ m^{-1}\ K^{-1}$)
λ_s	thermal conductivity of the horizontal plates ($W\ m^{-1}\ K^{-1}$)
$(\rho c)_f$	volumetric heat capacity of the fluid ($J\ m^{-3}\ K^{-1}$)
$(\rho c)_p$	volumetric heat capacity of porous saturated medium ($J\ m^{-3}\ K^{-1}$)
$(\rho c)_s$	effective volumetric heat capacity of the horizontal plates ($J\ m^{-3}\ K^{-1}$)
ϕ	heat capacity ratio $\phi = \frac{(\rho c)_p}{(\rho c)_f}$
ψ	stream function
ν	kinematic viscosity of fluid ($m^2\ s^{-1}$)

A linear stability analysis determining the onset of convection in a bounded rectangular cavity containing a fluid-saturated porous medium was performed by Kubitschek and Weidman [14] for insulated sidewalls, an isothermal upper surface, and a lower surface which is heated by forced convection and which therefore introduces the need for a Biot number, Bi. Numerical calculations of the critical Rayleigh number, Ra_c, were made over the range of Biot numbers, $10^{-4} \leqslant \mathrm{Bi} \leqslant 10^4$, and for cavity aspect ratios satisfying $0 \leqslant A \leqslant 5$. These computations cover all the effective lower surface heating conditions from the constant heat flux global limit, $Ra_c = 27.096$, which is found as $\mathrm{Bi} \to 0$, to the isothermal global limit, $Ra_c = 4\pi^2$ found as $\mathrm{Bi} \to \infty$. Marginal stability boundaries preferred cellular modes and disturbance temperature contours were displayed graphically.

A compilation of most of the pertinent information on the critical Rayleigh number and wavenumber for an infinite layer with different boundary conditions, (viz. open or impermeable; prescribed temperature or prescribed heat flux) may be found in Nield and Bejan [1] and is reproduced in Table 1. However, other aspects of this problem continue to attract substantial interest, as evidenced by the most recent papers by Rees and Tyvand [15] and Nield and Kuznetsov [16] concerning the effects of different types of heterogeneity on the onset of convection in a porous medium. Moreover, the onset and development of binary convection in a horizontal porous enclosure have been investigated by Mamou and Vasseur [17] and Charrier-Mojtabi et al. [18] using both linear and nonlinear perturbation theories.

The main interest of the present work lies in the fact that very few papers exist which consider the effect of the presence of horizontal bounding plates on the onset of convection. In an early paper Donaldson [19] considered a two-layer system where layer is impermeable, while Jang and Tsai [20] analyzed a three-layer system in which the middle layer is impermeable. Riahi [21], on the other hand, considered a weakly nonlinear analysis of what is, in effect, a pair of plates of infinite height. In the present paper the thermodynamic system includes both the porous cavity and its bounding surfaces which are heated by means of a uniform heat flux. We show that the stability threshold of the bulk (the saturated porous medium) cannot be dissociated from the boundary conditions due to conduction within the external plates bounding the saturated porous medium. Kubitschek and Weidman [14] consider that neither uniform temperature nor uniform heat flux boundary conditions are met easily in engineering practice, although close approximations to them may be realized in controlled laboratory experiments. Use is often made of a variable heat flux boundary condition involving the Biot number, Bi, to bridge the gap from uniform temperature to uniform heat flux. This imperfect boundary condition is sometimes referred to as forced convection heat transfer or Newtonian heating. We are led to believe that it is possible to obtain a uniform heat flux boundary condition more easily in a laboratory than a uniform temperature. But the use of intense forced convection may also ensure uniform temperature on the outer surfaces of the external plates bounding the porous medium only. If we take into account the heat transfer inside these plates, which is the aim of the present paper, then it is no longer necessary to introduce the Biot number.

The chief objective of our work, then, is to determine the effect on the stability properties of a horizontal porous layer of the presence of conducting surfaces bounding the porous layer both above and below. As such this provides a better approximation to how experiments are set up in the laboratory than does the usual fixed temperature or heat flux boundary conditions. In this paper particular attention is focussed upon the influence of the conductivity ratio and the thickness ratio.

Table 1
Critical Rayleigh number Ra_c and the critical wavenumber k_c, under various boundary conditions, mentioned by Nield and Bejan [1].

Lower surface	Upper surface	Ra_c	k_c
FST, IMP	FST, IMP	$4\pi^2$	π
FST, IMP	CHF, IMP	27.10	2.33
CHF, IMP	CHF, IMP	12	0
FST, IMP	FST, FREE	27.10	2.33
CHF, IMP	FST, FREE	17.65	1.75
FST, IMP	CHF, FREE	π^2	$\pi/2$
CHF, IMP	CHF, FREE	3	0

FST: fixed surface temperature, IMP: impermeable and CHF: constant heat flux.

2. Mathematical formulation

The configuration considered in this study is that of a horizontal porous layer of uniform thickness, H, width, L, permeability, K and porosity, φ, and which is filled with a pure fluid (see Fig. 1). The origin of the coordinate system is located at the bottom of the porous cavity with x' and y' being the horizontal and vertical coordinates, respectively. This cavity is placed between two metal

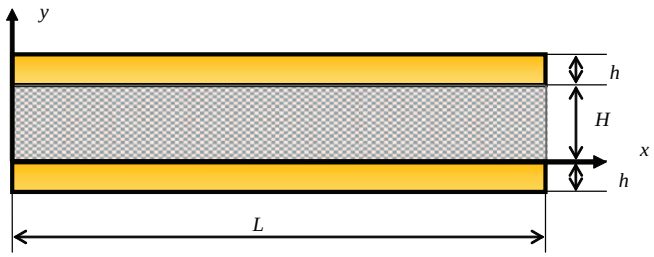

Fig. 1. Saturated porous medium of height H and length L bounded by two horizontal plates of height h. The upper and lower surfaces of the system are subject to a uniform heat flux. The vertical sidewalls are assumed to be perfectly insulated.

plates of uniform thickness, h. Neumann boundary conditions for temperature (i.e. fixed heat flux) are applied on the outer horizontal surfaces of the layer at $y' = -h$ and at $y' = H + h$. All the boundaries are impermeable and we consider a rectangular cavity with high aspect ratio $A = L/H$.

The stability analysis is undertaken for the general case for which the aspect ratio is infinite. This is not a restrictive condition, as is well-known for a Darcy medium, because the sidewall boundary conditions are also satisfied at the vertical boundaries of the cell pattern. The cavity is filled with a porous medium and is saturated by a pure fluid. The impermeable horizontal walls ($y = -h$, $y = H + h$) are subjected to a uniform heat flux per unit area, q'. The vertical walls ($x = 0, x = L$) are impermeable and adiabatic. All the boundaries are assumed to be rigid. We also assume that the porous medium is isotropic and homogeneous, that Darcy's law is valid, and that the Oberbeck–Boussinesq approximation is applicable: the thermophysical properties of the pure fluid are therefore considered to be constant except for the density in the buoyancy term, which is taken to vary linearly with the local temperature:

$$\rho = \rho_0(1 - \beta(T' - T_i)). \tag{1}$$

Here β is the coefficient of thermal expansion of the fluid, T' is the dimensional temperature and T_i corresponds to the reference state. We also use the other standard assumptions such as local thermal equilibrium between the phases and negligible viscous dissipation.

Thus the governing conservation equations for mass, momentum and energy for the bulk are:

$$\begin{cases} \nabla^2\psi' = -\frac{gK\beta}{\nu}\frac{\partial}{\partial x'}T_2', \\ (\rho c)_p \frac{\partial T_2'}{\partial t'} + (\rho c)_f \mathbf{V}'.\nabla T_2' = \lambda_p \nabla^2 T_2', \end{cases} \tag{2}$$

where $\mathbf{V}'$ is the Darcy velocity, T_2' the temperature inside the porous bulk, g the gravitational acceleration, ν the kinematic viscosity, $(\rho c)_p$ and $(\rho c)_f$ are the respective heat capacities of the saturated porous medium and the fluid, λ_p is the effective thermal conductivity of the saturated porous medium, and ψ' is the stream function. As usual the equation of continuity is satisfied by introducing the streamfunction according to: $u' = \partial\psi'/\partial y'$ and $v' = -\partial\psi'/\partial x'$.

For the two plates bounding the porous medium, we have:

$$(\rho c)_s \frac{\partial T_1'}{\partial t'} = \lambda_s \nabla^2 T_1' \quad \text{and} \quad (\rho c)_s \frac{\partial T_3'}{\partial t'} = \lambda_s \nabla^2 T_3', \tag{3}$$

where T_1' and T_3' are the temperatures inside the lower and upper plates, respectively, and $(\rho c)_s$ and λ_s are the heat capacity and the thermal conductivity of the solid material. We have assumed that bounding plates are made from the same material and are of identical thicknesses.

The boundary conditions applied on the horizontal boundaries of the system are uniform fluxes of heat per unit area, q'. It is assumed that the vertical walls of the cavity are thermally well insulated and impermeable. Thus we have:

– for the bottom plate,

$$\text{for } y' = -h, \quad -\lambda_s \frac{\partial T_1'}{\partial y'} = q';$$

$$\text{for } y' = 0, \quad \lambda_s \frac{\partial T_1'}{\partial y'} = \lambda_p \frac{\partial T_2'}{\partial y'};$$

– for the porous bulk,

$$\text{for } y' = 0, \quad T_1' = T_2';$$
$$\text{for } y' = H, \quad T_2' = T_3';$$

– for the top plate,

$$\text{for } y' = H, \quad \lambda_p \frac{\partial T_2'}{\partial y'} = \lambda_s \frac{\partial T_3'}{\partial y'};$$

$$\text{for } y' = H + h, \quad -\lambda_s \frac{\partial T_3'}{\partial y'} = q'.$$

The reference scales are H for length, $H^2/(\lambda_p/(\rho c)_p)$ for time, a/H for the velocity, where $a = \lambda_p/(\rho c)_f$ is the effective thermal diffusivity, a for the stream function, and $\Delta T' = q'H/\lambda_p$ for the temperature. In terms of the above definitions, the dimensionless governing equations are given by

$$\begin{cases} \nabla^2\psi = -Ra\frac{\partial}{\partial x}T_2 \\ \phi\frac{\partial T_2}{\partial t} + \mathbf{V}\cdot\nabla T_2 = \nabla^2 T_2 \\ \frac{\partial T_1}{\partial t} = \alpha\nabla^2 T_1 \\ \frac{\partial T_3}{\partial t} = \alpha\nabla^2 T_3 \end{cases} \tag{4}$$

where φ and α represent the heat capacity ratio, $\phi = \frac{(\rho c)_p}{(\rho c)_f}$, and the thermal diffusivity ratio, $\alpha = \frac{a_s}{a}$, respectively, and a_s is the thermal diffusivity of the solid plates. The corresponding dimensionless boundary conditions are:

$$\begin{aligned} &\text{for } y = -\delta, \quad \frac{\partial T_1}{\partial y} = -\frac{\lambda_p}{\lambda_s} = -1/d; \\ &\text{for } y = 0, \quad \frac{\partial T_1}{\partial y} = \frac{\partial T_2}{\partial y}/d, \quad T_1 = T_2, \ \psi = 0; \\ &\text{for } y = 1, \quad \frac{\partial T_3}{\partial y} = \frac{\partial T_2}{\partial y}/d, \quad T_2 = T_3, \ \psi = 0; \\ &\text{for } y = 1 + \delta, \quad \frac{\partial T_3}{\partial y} = -1/d; \end{aligned} \tag{5}$$

The problem under consideration may now be seen to depend on six non-dimensional parameters: the thermal Rayleigh number, $Ra = Kg\beta H\Delta T'/(a_p\nu)$, where the temperature scale is $\Delta T' = \frac{q'H}{\lambda_p}$, the heat capacity ratio, $\phi = \frac{(\rho c)_p}{(\rho c)_f}$, the thermal diffusivity ratio, $\alpha = \frac{a_s}{a}$, the thermal conductivity ratio, $d = \frac{\lambda_s}{\lambda_p}$, the aspect ratio $\delta = \frac{h}{H}$ and the aspect ratio of the porous bulk, $A = L/H$. In the present study the intensity of the thermal buoyancy forces is expressed solely in terms of the parameter, Ra.

3. Linear stability of the equilibrium solution

3.1. The general analysis for O(1) wavenumbers

It is straightforward to show that there exists an equilibrium solution characterized by:

$$\begin{aligned} &\mathbf{V} = 0; \quad T_{1,0} = -y/d + T_0; \quad T_{2,0} = T_0 - y, \\ &T_{3,0} = (1 - y)/d + T_0 - 1, \end{aligned} \tag{6}$$

where T_0 is an arbitrary constant temperature. In order to analyze the stability of this equilibrium solution, we first introduce the

perturbation of the stream function, ψ, and perturbations of the temperatures, namely, θ_1, θ_2 and θ_3. We assume that the perturbations (ψ, θ_1, θ_2, θ_3) are of asymptotically small amplitude, and we obtain the following linearized equations:

$$\begin{cases} \nabla^2\psi + Ra\frac{\partial}{\partial x}\theta_2 = 0, \\ \phi\frac{\partial\theta_2}{\partial t} - \nabla^2\theta_2 - v = 0, \\ \frac{\partial\theta_1}{\partial t} - \alpha\nabla^2\theta_1 = 0, \\ \frac{\partial\theta_3}{\partial t} - \alpha\nabla^2\theta_3 = 0 \end{cases} \tag{7}$$

with the associated boundary conditions:

$$\begin{aligned} &\text{for } y = -\delta, \quad \frac{\partial\theta_1}{\partial y} = 0; \\ &\text{for } y = 0, \quad \frac{\partial\theta_1}{\partial y} = \frac{\partial\theta_2}{\partial y}/d, \quad \theta_1 = \theta_2, \ \psi = 0; \\ &\text{for } y = 1, \quad \frac{\partial\theta_3}{\partial y} = \frac{\partial\theta_2}{\partial y}/d, \quad \theta_2 = \theta_3, \ \psi = 0; \\ &\text{for } y = 1+\delta, \quad \frac{\partial\theta_3}{\partial y} = 0. \end{aligned} \tag{8}$$

The perturbation quantities are chosen as follows:

$$(\psi, \theta_1, \theta_2, \theta_3) = (\tilde{\psi}, \tilde{\theta}_1, \tilde{\theta}_2, \tilde{\theta}_3)(y)\exp(ikx + \sigma t) + \text{c.c.}, \tag{9}$$

where k is the wavenumber in the horizontal (x) direction, $i^2 = -1$, and σ is the temporal exponential growth rate of the perturbation.

Appendix A shows that the principle of exchange of stabilities applies for this system, and therefore σ is always real. Therefore we may study the instability via a stationary bifurcation for which $\sigma = 0$. Substitution of (9) into Eqs. (7) leads to the homogeneous differential system:

$$\begin{cases} (D^2 - k^2)\tilde{\psi}(y) + ikRa\tilde{\theta}_2(y) = 0, \\ (D^2 - k^2)\tilde{\theta}_2(y) - ik\tilde{\psi}(y) = 0, \\ (D^2 - k^2)\tilde{\theta}_1(y) = 0, \\ (D^2 - k^2)\tilde{\theta}_3(y) = 0, \end{cases} \tag{10}$$

where $D = \partial/\partial y$. On elimination of $\tilde{\psi}$ from the system (10), the following linear system is obtained:

$$(D^2 - k^2)^2\tilde{\theta}_2(y) - k^2Ra\tilde{\theta}_2(y) = 0, \tag{11a}$$

$$(D^2 - k^2)\tilde{\theta}_1(y) = 0, \tag{11b}$$

$$(D^2 - k^2)\tilde{\theta}_3(y) = 0, \tag{11c}$$

with the associated boundary conditions:

$$\begin{aligned} &\text{for } y = -\delta, \quad \frac{\partial\tilde{\theta}_1}{\partial y} = 0; \\ &\text{for } y = 0, \quad \frac{\partial\tilde{\theta}_1}{\partial y} = \frac{\partial\tilde{\theta}_2}{\partial y}/d, \quad \tilde{\theta}_1 = \tilde{\theta}_2, \quad (D^2 - k^2)\tilde{\theta}_2 = 0; \\ &\text{for } y = 1, \quad \frac{\partial\tilde{\theta}_3}{\partial y} = \frac{\partial\tilde{\theta}_2}{\partial y}/d, \quad \tilde{\theta}_2 = \tilde{\theta}_3, \quad (D^2 - k^2)\tilde{\theta}_2 = 0; \\ &\text{for } y = 1+\delta, \quad \frac{\partial\tilde{\theta}_3}{\partial y} = 0. \end{aligned} \tag{12}$$

The general solution of the fourth order ordinary differential equation in Eq. (11) may be written as a combination of four independent functions whose expression depends on the sign of the quantity, $k^2 - k\sqrt{Ra}$. When $Ra < k^2$, the equations have no nonzero solution in this case. When $Ra > k^2$, the solution of Eq. (11) is:

$$\begin{aligned} \tilde{\theta}_2(y) = {} & A\cosh(\sqrt{k^2 + k\sqrt{Ra}}y) + B\sinh(\sqrt{k^2 + k\sqrt{Ra}}y) \\ & + C\cos(\sqrt{k\sqrt{Ra} - k^2}y) + D\sin(\sqrt{k\sqrt{Ra} - k^2}y). \end{aligned}$$

The solution obtained depends on the four arbitrary constants A, B, C and D. The general solutions of the second order ordinary differential equations in Eq. (11) may now be written in the form:

$$\tilde{\theta}_1(y) = E\cosh(ky) + F\sinh(ky),$$

$$\tilde{\theta}_3(y) = G\cosh(ky) + M\sinh(ky),$$

where E, F, G and M are also arbitrary. When we assume that this general solution satisfies the eight boundary conditions given in Eq. (12), we obtain eight homogeneous linear algebraic equations and eight unknowns corresponding to the eight constants. This system has a non-trivial solution if the associated matrix determinant, $\det(Ra(k), k, \delta, d)$ is equal to zero. The full expression of this determinant was obtained using the package, Maple. Once we have calculated the determinant, we may obtain the relation between the Rayleigh number, the wavenumber, the aspect ratio δ and the thermal conductivity ratio d. The analytical dispersion relation is given by:

$$\begin{aligned} & k^2\sinh(R_1)\sin(R_2)(2d^2\tanh(k\delta)^2 + 1) + 2kd\tanh(k\delta) \\ & \quad \times (R_2\sinh(R_1)\cos(R_2) + R_1\cosh(R_1)\sin(R_2)) \\ & \quad + R_1R_2(\cosh(R_1)\cos(R_2) - 1) = 0 \end{aligned} \tag{13}$$

where:

$$R_1 = \sqrt{(k + \sqrt{Ra})k} \quad \text{and} \quad R_2 = \sqrt{(\sqrt{Ra} - k)k}$$

We note that a slightly different method of analysis leading to the same dispersion relation may be obtained by 'replacing' the detailed solution in the solid bounding plates by equivalent boundary conditions for the porous layer; see Appendix B for more precise details.

Figs. 2 and 3 show some typical neutral curves which have been obtained using Eq. (13). In Fig. 2 are displayed curves for the case, $\delta = 1$, which corresponds to bounding plates which are much thicker than would typically be used in experimental work. The lowest curve has a minimum at $k = 0$ and the corresponding value of the Rayleigh number is approximately 12, which is the well-known result for the classical porous layer with constant heat flux boundaries. In this case the conductivity ratio, d, is small which means that the bounding plates are highly sensitive to the cellular pattern in the porous layer.

The opposite extreme would be for very large values of d when the bounding plates are highly conducting. Thus the plates will

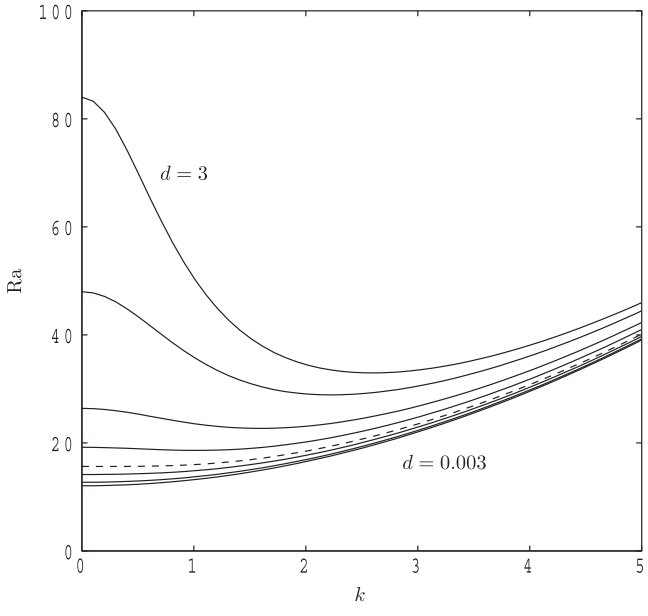

Fig. 2. Neutral curves for the case $\delta = 1$, where d takes the following values: 0.003 (lowest curve), 0.03, 0.09, 0.1520775, 0.3, 0.6, 1.5 and 3 (uppermost curve). The dashed line corresponds to $d = 0.1520775$ for which the neutral curve has a quartic minimum at $k = 0$.

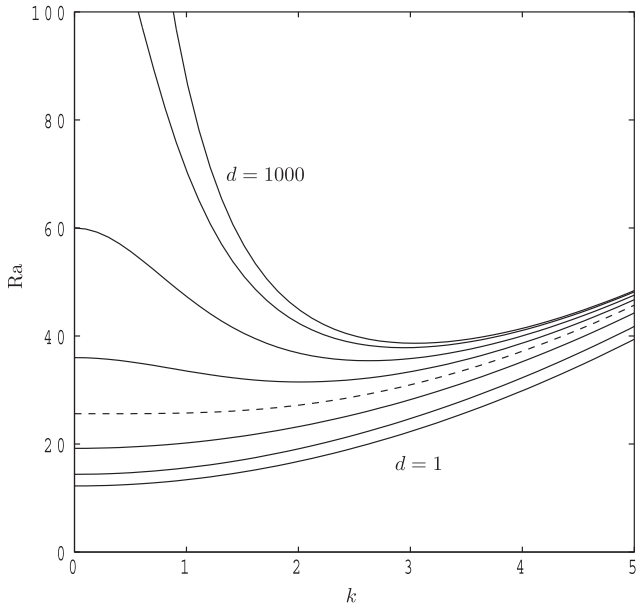

Fig. 3. Neutral curves for the case $\delta = 0.01$, where d takes the following values: 1 (lowest curve), 10, 30, 57.573028, 100, 200, 500 and 1000 (uppermost curve). The dashed line corresponds to $d = 57.573028$ for which the neutral curve has a quartic minimum at $k = 0$.

equilibrate quickly to a uniform temperature, and therefore the full system will mimic the classical constant temperature surface. The approach to this state may be seen in Fig. 2 as d increases. The minimum value of Ra rises and the associated critical wavenumber ceases to take zero values and is tending towards π.

There exists a transitional case between the two extremes where local maximum at $k = 0$ and the local minimum when $k > 0$ approach one another as d decreases. For $\delta = 1$ the two critical points merge at $k = 0$ to form a quartic minimum when $d = 0.1520775$; this case is marked by a dashed curve in Fig. 2. Thus the critical Rayleigh number has a nonzero critical wavenumber when d takes values larger than this, a zero one when it takes smaller values. Further aspects of this transition are given later.

Fig. 3 shows the equivalent situation for bounding plates of thickness $\delta = 0.01$. The general trend is as given in Fig. 2, but the corresponding values of d are much larger. Here, the transitional curve with the quartic minimum corresponds to $d = 57.573028$. This pair of parameter values would be quite typical of an experiment where the bounding plates are highly conducting but quite thin. Given that small relative changes to d quite clearly make quite large quantitative and qualitative differences to the critical Rayleigh number and the identity of the onset wavenumber, it is clear that one would need to take great care in choosing one's materials for an experimental study.

It turns out not to be necessary to present further curves, especially if one is interested in modelling experimental work, i.e. for cases where the bounding plates are thin. The mathematical properties of the dispersion relation given in (13) are such that Fig. 3 will be reproduced almost exactly for other small values of δ as long as the product $d\delta$ is conserved. For example, the analogous set of curves for $\delta = 0.001$ will be almost exactly those given in Fig. 2 if the chosen values of d are 10 times those displayed in Fig. 2. To show this, if we assume that $\delta \ll 1$, but that $k = O(1)$, then Eq. (13) reduces to

$$k^2 \sinh(R_1)\sin(R_2)(2k^2d^2\delta^2 + 1) + 2k^2 d\delta(R_2 \sinh(R_1)\cos(R_2) + R_1 \cosh(R_1)\sin(R_2)) + R_1R_2(\cosh(R_1)\cos(R_2) - 1) = 0,$$

which is a function of Ra, k, and $d\delta$ (rather than d and δ separately). We note that this general result, which holds formally when $\delta \ll 1$, may be shown numerically to be quite accurate even when δ is as large as 0.1.

It is now possible to determine the critical Rayleigh number by minimizing each curve over values of k. This was done using a straightforward two-dimensional Newton–Raphson routine which simultaneously finds Ra and minimizes with respect to the wavenumber. The results of our computations are summarized in Figs. 4 and 5, which show Ra_c and k_c, respectively.

In Fig. 4 we have chosen to display the critical Rayleigh number as a function of δ for a chosen set of values of d. Each curve is split into two distinct regions, the first of which corresponds to relatively small values of δ, and is the regime within which the critical wavenumber is zero. In this regime the 'curve' is a straight line, and this is shown mathematically in the next subsection. The second region corresponds to nonzero values of the critical wavenumber. As δ increases, each curve tends towards a horizontal asymptote. Physically this means that any x-dependent pattern which is caused by the cells within the porous layer will have decayed within the bounding plates and the temperature at the bounding surfaces is uniform. Therefore the stability criterion is independent of any further increase in the thickness of the bounding plates. Once more we see that high conductivity ratios lead the system to mimic the classical constant temperature boundary condition scenario more closely.

The corresponding critical wavenumbers are shown in Fig. 5. The transition between the zero and nonzero critical wavenumber regimes is very clear. When d is sufficiently large, then k_c is close to π, except for those situations where the bounding plates are sufficiently thin.

3.2. The limiting case of long-wave disturbances $k \approx 0$

The case of long-wave disturbances (for which the wavenumber, k, is at or close to zero) may be studied analytically using the dispersion relation, (13), by developing a regular perturbation expansion using k as a small parameter. In our case, we expand the determinant in the vicinity of $k = 0$ using Maple to obtain:

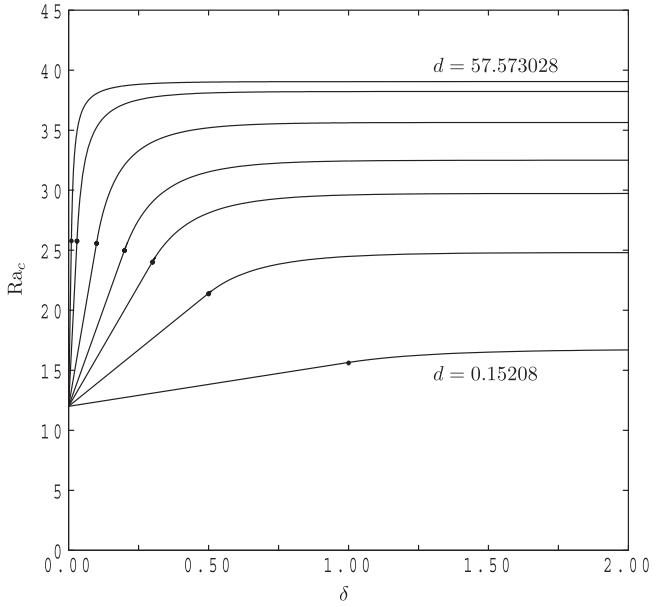

Fig. 4. Globally minimized neutral curves for Ra_c as functions of δ for the following values of d: 57.573028, 19.16802, 5.67240, 2.71048, 1.67401, 0.78432 and 0.15208. These values have been chosen so that there exists a quartic minimum when $\delta = 0.01$, 0.03, 0.1, 0.2, 0.3, 0.5 and 1, respectively; the locations of the quartic minima are shown by the bullet symbols. The neutral curves to the left of the symbols form straight lines in accordance with Eq. (15).

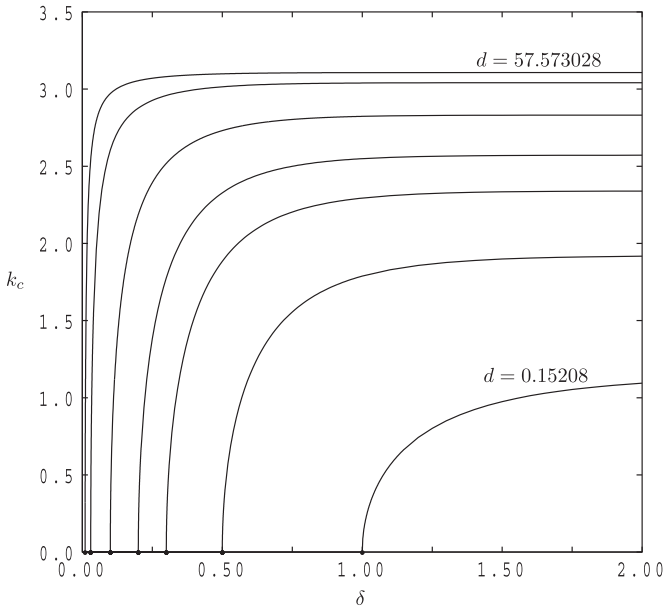

Fig. 5. Wavenumbers corresponding to the curves shown in Fig. 4. The bullet symbols again display the parameter set for which the neutral curve has a quartic minimum.

$$\det(Ra(k), k, \delta, d) = F_1(Ra_0, \delta, d)k^3 + F_2(Ra_0, Ra_2, \delta, d)k^5 + O(k^7),$$

where

$$Ra = Ra_0 + Ra_2 k^2 + \cdots$$

has also been used. Thus we obtain the following expression for the first term,

$$F_1(Ra_0, \delta, d) = Ra_0 - 12 - 24d\delta. \tag{14}$$

However, the full expression for $F_2(Ra_0, Ra_2, \delta, d)$ is very considerably more complicated, and it will be given later after some simplification. When we set the $O(k^3)$ term in the determinant to zero, it leads to:

$$Ra_0 = 12(1 + 2d\delta). \tag{15}$$

This equation confirms our previous statement that the critical Rayleigh number is a linear function of δ for suitable ranges of values of δ, as shown in Fig. 4. When Eq. (15) is substituted into the expression for $F_2(Ra_0, Ra_2, \delta, d)$, then we obtain:

$$Ra_2(\delta, d) = -8d\delta^3 - \frac{204}{35}d^2\delta^2 + \frac{48}{35}d\delta + \frac{8}{7}. \tag{16}$$

Given the form of Eq. (15), we note that the critical Rayleigh number, Ra_0 corresponding to the long wave, $k = 0$, also depends only on the product $d\delta$. In domains that would be used in experimental work, these two parameters would exhibit the following typical ranges of values: $\delta \in [0.01, 2]$ and $d \in [10^{-4}, 1]$.

As mentioned earlier, the variation of Ra given by (13) exhibits a single minimum which is either at $k_c = 0$, or else at nonzero values. When the latter occurs, Ra has a local maximum value at $k = 0$. The regions in which the two behaviours arise are delimited by the case where $Ra_2 = 0$, which corresponds to when the neutral curve has a quartic minimum. From Eq. (16) we deduce that this transitional case occurs when,

$$\delta d = f(\delta) = -\frac{35}{51}\delta^2 + \frac{\sqrt{1225\delta^4 - 420\delta^2 + 546}}{51} + \frac{2}{17}. \tag{17}$$

The dependence of d and δ upon one another at the quartic point is shown in Fig. 6. Points above the curve are those for which the critical wavenumber is nonzero, while those below the curve have a zero critical wavenumber. It is also possible to use (17) to show that

$$d \approx \left(\frac{\sqrt{546}}{51} + \frac{2}{17}\right)\delta^{-1} \quad \text{when } \delta \ll 1$$

and

$$d \approx \frac{1}{7\delta^3} \quad \text{when } \delta \gg 1.$$

Then we can deduce that the critical Rayleigh number corresponding to $k_c = 0$ is:

$$Ra_{c_0} = 12(1 + 2d\delta) = 12(1 + 2f(\delta)). \tag{18}$$

In the small-δ limit this expression for Ra_c yields $Ra_{c0_{\max}} \cong 25.82$, which may be seen in Fig. 4. The corresponding minimum arises when $\delta \to \infty \Rightarrow f(\delta) \to 0$ and hence $Ra_{c_0} \to 12$; this may also be seen in Fig. 4 as the trend exhibited by the bullet symbols when δ becomes large.

4. Analytical solution of the unicellular flow

For the limiting case of a shallow cavity, for which $A \gg 1$, we may use the parallel flow approximation [22,23] to determine the flow and temperature fields. The basic state is denoted by the subscript, "b", and it may be written as follows:

$$\psi = \psi_b(y), \quad T_{1b} = Cx + \theta_1(y) \quad T_{2b} = Cx + \theta_2(y)$$
$$T_{3b} = Cx + \theta_3(y). \tag{19}$$

On using the assumptions already mentioned and the corresponding boundary conditions, the stationary stream function and the temperature fields corresponding to the three regions are given by,

$$\begin{cases} \psi_b = \frac{1}{2}RaC(y - y^2), \\ T_{1b} = Cx - y/d + \beta, \\ T_{2b} = Cx + \frac{1}{2}RaC^2\left(\frac{1}{2}y^2 - \frac{1}{3}y^3\right) - y + \beta, \\ T_{3b} = Cx - y/d + \frac{1}{12}RaC^2 + \beta + 1/d - 1. \end{cases} \tag{20}$$

The value, β, is arbitrary, due to the use of Neumann boundary conditions, but the constant, C is currently unknown. However, its

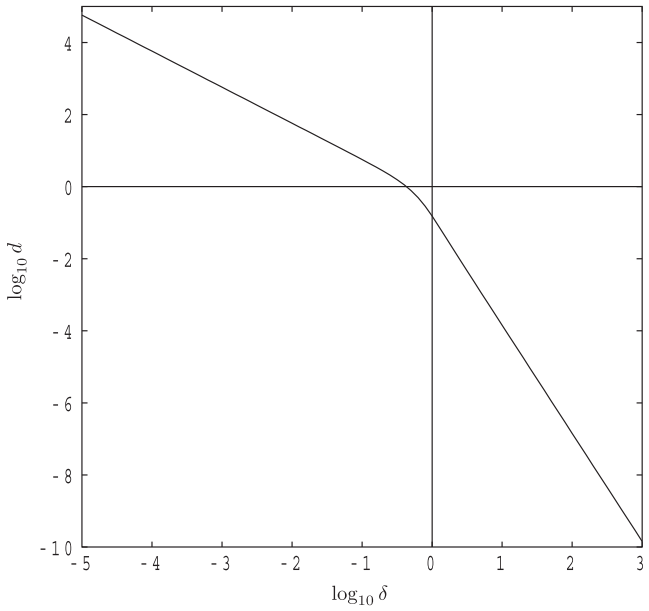

Fig. 6. Showing the locus of quartic points in (δ, d)-space, as given in Eq. (17). Regions below the curve correspond to situations for which $k_c = 0$, and regions above to where $k_c \neq 0$. Note that $d \sim 0.57582/\delta$ when $\delta \ll 1$ and $d \sim 1/(7\delta^3)$ when $\delta \gg 1$.

value may be determined by imposing zero heat flux across any transversal section of the cell, and this yields:

$$\int_{-\delta}^{0} -d\frac{\partial T_{1b}}{\partial x}dy + \int_{0}^{1} -\frac{\partial T_{2b}}{\partial x}dy + \int_{1}^{1+\delta} -d\frac{\partial T_{3b}}{\partial x}dy + \int_{0}^{1} T_{2b}\frac{\partial \psi}{\partial y}dy = 0. \quad (21)$$

On applying Eq. (21) we deduce the following values of the parameter, C:

$$C_1 = 0, \quad C_2 = \frac{\sqrt{10}}{Ra}\sqrt{Ra - 12 - 24d\delta},$$
$$C_3 = -\frac{\sqrt{10}}{Ra}\sqrt{Ra - 12 - 24d\delta}. \quad (22)$$

A few remarks may be made concerning these three expressions for C in the temperature field. The expression under the root sign must be positive, which means that $Ra > 12(1 + 2d\delta)$. This value of Ra corresponds to the critical Rayleigh number for the onset of long-wavelength convection obtained above. It is also clear that C_2 is positive and C_3 is negative; this reflects the fact the flow may be either clockwise or anticlockwise, and the basic unicellular state which is realized in practice depends on the initial conditions. A similar result, giving the analytical value of the critical Rayleigh number, was obtained by Elhajjar et al. [22] in the case of double diffusive convection. The value $C_1 = 0$ corresponds to the zero-flow diffusive state.

From Eqs. (20) and (22) we may also deduce that the intensity of the flow increases as $\sqrt{Ra - Ra_c}$. On the other hand, the horizontal temperature gradient rises initially as Ra increases from the critical value, $Ra_c = 12(1 + 2\delta d)$, until it achieves its maximum value at $Ra = 2Ra_c$. Finally, we note that this solution may be regarded as being a fully nonlinear solution, even though the equations which have been solved are linear. This solution is valid whenever $Ra > Ra_c$ although it is outside of the scope of this paper to determine whether the solution is realized in practice for all values of Ra.

5. Linear stability within a finite cavity

Because experimental work must take place with a finite cavity, even if its aspect ratio, A, is large, there will be finite aspect ratio

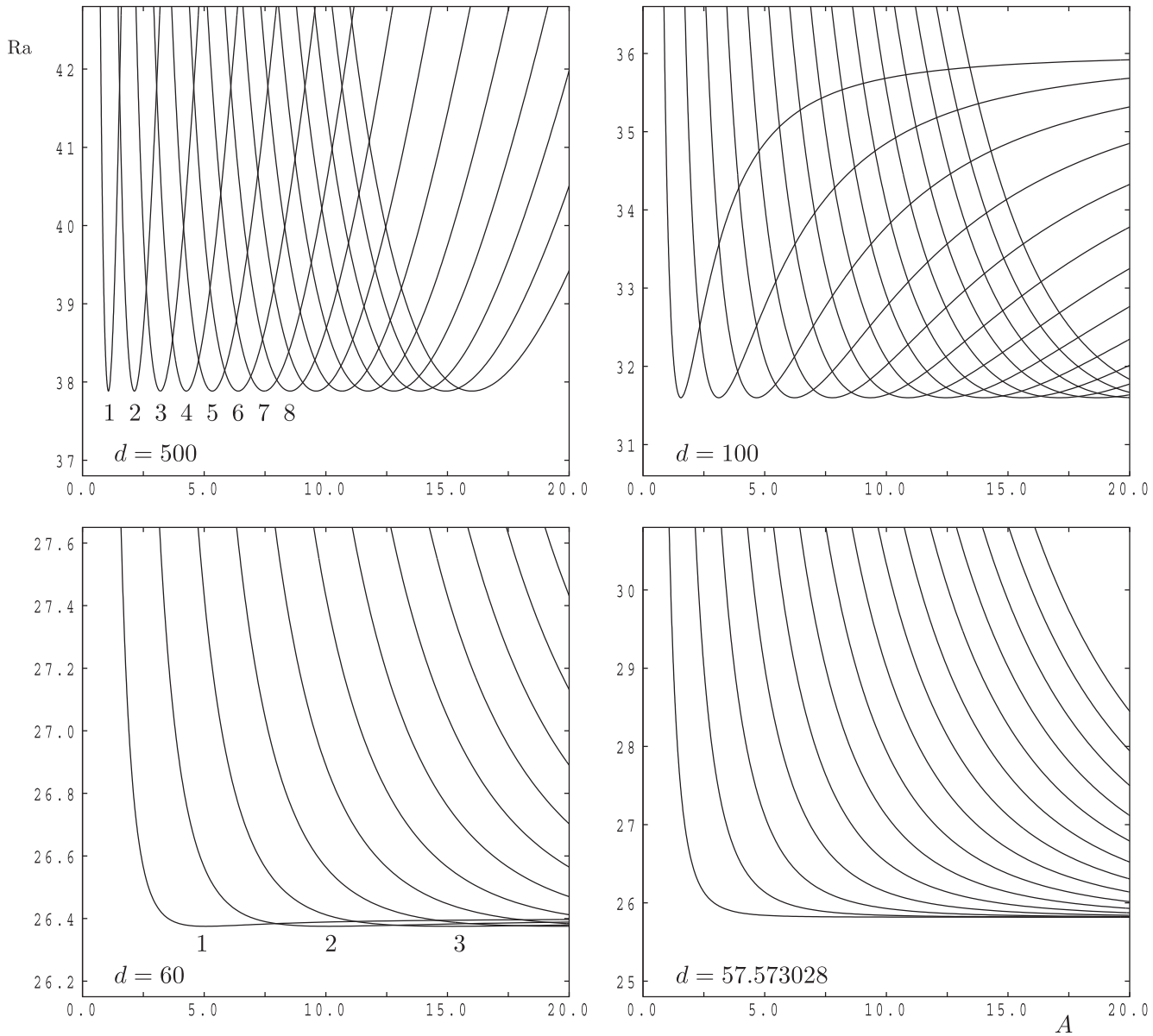

Fig. 7. Neutral curves for discrete modes within a cavity of aspect ratio (length), A. In each frame, the left hand curve corresponds to the neutral curve for a 1-cell mode, the next to a 2-cell mode and so on, as indicated in the left hand frames. We have taken $\delta = 0.01$ and the values of d are given in the frames themselves.

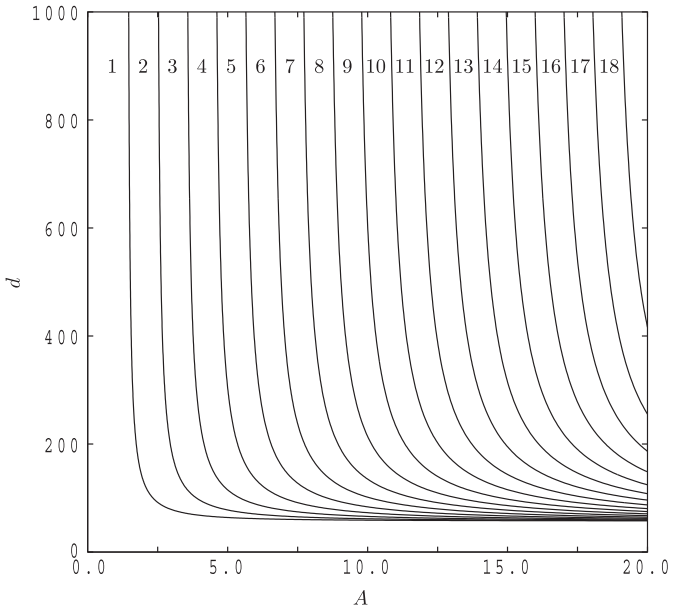

Fig. 8. Displaying the critical mode in terms of the number of cells as a function of the cavity width, A, and the conductivity ratio, d, when $\delta = 0.01$. The region between each pair of lines corresponds to an onset mode with the number of cells indicated.

effects which will modify slightly some of the above analysis. In particular, the zero wavenumber cell will not appear, but it will be replaced by a unicellular motion within the cavity. When the critical wavenumber for the infinitely long cavity is nonzero, it too may not appear because the length of the cavity is such that a whole number of cells will not fit within it. Therefore it is important to gain some understanding of what might be observed in practice when the layer has a finite aspect ratio.

As mentioned earlier, when flow is governed by Darcy's law and when the sidewalls are insulated, the conditions which arise at a cell boundary are identical to those which arise at a sidewall, and therefore all solutions which exist in an infinitely long cavity may also exist in a finite cavity, but only if they fit into the available space.

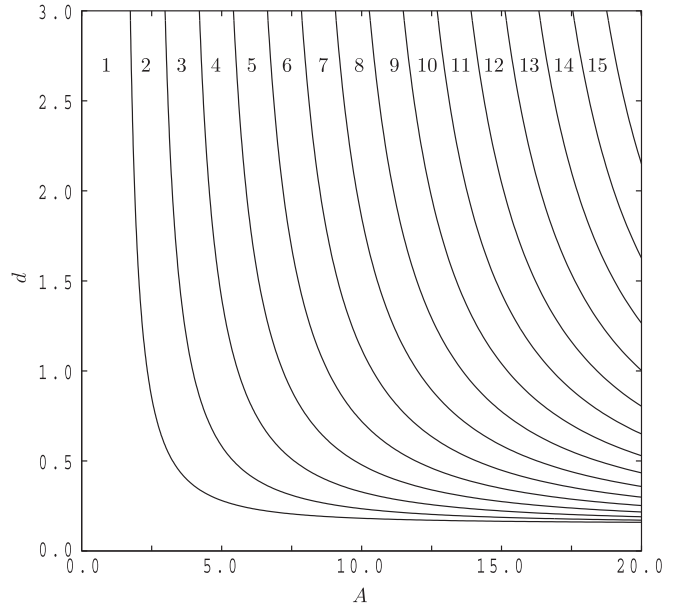

Fig. 9. Displaying the critical mode in terms of the number of cells as a function of the cavity width, A, and the conductivity ratio, d, when $\delta = 1$. The region between each pair of lines corresponds to an onset mode with the number of cells indicated.

Figs. 7 and 8 illustrate some typical cases, and correspond to thin plates for which $\delta = 0.01$. Fig. 7 shows the neutral curves for four different values of d as a function of the aspect ratio of the cavity, rather than the wavenumber. There are now multiple curves, each of which correspond to a different number of cells within the cavity. When $d = 500$, which is a relatively large value, the critical wavenumber is close to π. Therefore the number of cells which fit into the cavity is very roughly the closest integer to the aspect ratio of the cavity. However, as d decreases, the critical wavenumber becomes smaller, and therefore the range of values of the aspect ratio over which the preferred number of cells does not change increases. This is clearly illustrated by comparing the $d = 500$, $d = 100$ and $d = 60$ subframes of Fig. 7. Eventually, as d decreases sufficiently, the quartic point is reached, and when d takes this value or smaller values, then there is only one preferred pattern, namely a single cell flow. A summary of the progressive transition from rapid changes in the identity of the preferred mode to the small-d situation when the single cell is always preferred at onset, are shown in Fig. 8, for $\delta = 0.01$ and in Fig. 9 for $\delta = 1$, for the sake of comparison.

6. Conclusion

We have conducted a theoretical study of the onset of natural convection in an isotropic, saturated porous layer sandwiched between two rigid, horizontal impermeable but conducting surfaces. This has led to the following main result.

For all plate thicknesses the stability properties of the composite layer vary from that of the classical constant temperature Horton–Rogers–Lapwood problem, for which critical Rayleigh number and wavenumber are equal to $4\pi^2$ and π, respectively, and which corresponds to very highly conducting plates, through to the analogous constant heat flux scenario where the critical wavenumber is zero, which corresponds to a poorly conducting pair of bounding plates. The critical Rayleigh number in the latter case is given by Eq. (15). The transition from one extreme to the other takes place via a neutral curve with a quartic minimum at zero wavenumber.

From a practical point of view we have shown that it is essential to determine the combined effect of the relative thickness of the bounding plates and the ratio of the conductivities of the plates and the saturated porous medium. In some regions of parameter space a small change in one of these values will cause large qualitative and quantitative changes in the stability characteristics. Physically this arises because the varying heat flux which arises from the presence of convective motions in the porous layer may or may not get redistributed by horizontal conduction within the bounding plates.

A further practical implication is that it is possible to determine the effective conductivity of the porous medium by engineering a situation wherein the critical wavenumber is zero. In such a situation the critical Rayleigh number is given by Eq. (15), i.e. $Ra_0 = 12(1 + 2d\delta)$. Given that the thickness and conductivity of the bounding plates will be known to a good accuracy, then, once the critical Rayleigh number has been determined experimentally, it will be straightforward to calculate d and, in turn, the conductivity of the porous medium. In practice, an experimental rig will be finite in length, and so a unicellular pattern with a small wavenumber will be generated. The terms (14) and (16) in the small-k perturbation expansion of the dispersion relation, or even the dispersion relation itself, may be used together with a Newton–Raphson method for determining d.

Acknowledgements

The authors would like to thank the anonymous referees for their comments which have served to improve the presentation of the paper.

Appendix A. Showing the absence of oscillatory instability

If the principle of exchange of stabilities is to be valid, then it is necessary to show that σ must be real. On multiplying the first equation of the system (7) by ψ^*, the complex conjugate of ψ and integrating from $y = 0$ to $y = 1$, and, similarly, multiplying the second equation of the system (7) by θ_2^* and integrating from $y = 0$ to $y = 1$, we obtain,

$$\int_0^1 (|\psi'|^2 + k^2|\psi|^2)dy = Raik\int_0^1 \theta_2\psi^* dy, \tag{A.1a}$$

$$\int_0^1 (|\theta_2'|^2 + k^2|\theta_2|^2)dy + \sigma\int_0^1 |\theta_2|^2 dy - \left[\theta_2^*\theta_2'\right]_0^1 = -Raik\int_0^1 \theta_2^*\psi dy. \tag{A.1b}$$

On taking the complex conjugate of the second equation of (A.1b),

$$\int_0^1 (|\theta_2'|^2 + k^2|\theta_2|^2)dy + \sigma^*\int_0^1 |\theta_2|^2 dy - \left[\theta_2\theta_2'^*\right]_0^1 = +Raik\int_0^1 \theta_2\psi^* dy, \tag{A.2}$$

(A.2) and (A.1a) may be combined by eliminating the cross product terms to give,

$$\int_0^1 (|\theta_2'|^2 + k^2|\theta_2|^2)dy + \sigma^*\int_0^1 |\theta_2|^2 dy - \left[\theta_2\theta_2'^*\right]_0^1 = \int_0^1 (|\psi'|^2 + k^2|\psi|^2)dy. \tag{A.3}$$

After solving equation (11b) using the boundary condition (12) we deduce the following relation coupling the value of θ_2 and its derivative:

$$\theta_2' = kd\tanh(k\delta)\theta_2 \quad \text{for } y = 0 \quad \text{and}$$
$$\theta_2' = -kd\tanh(k\delta)\theta_2\cdots \quad \text{for } y = 1. \tag{A.4}$$

Therefore: $\left[\theta_2\theta_2'^*\right]_0^1 = -2kd\tanh(k\delta)\left[\theta_2\theta_2^*\right]_0^1 = -2kd\tanh(k\delta)\left[|\theta_2|^2\right]_0^1$.

Since all the integrals in (A.3) and the term, $\left[\theta_2\theta_2'^*\right]_0^1$ are real, then σ^* must also be real. We conclude that imaginary part of σ is equal 0, so there is no oscillatory instability for this problem.

Appendix B. Replacing the perturbation solutions in the bounding plates by an equivalent set of boundary conditions for the porous layer

The perturbation equation for the lower bounding plate is given in (11) and is,

$$(D^2 - k^2)\tilde{\theta}_1 = 0, \tag{B.1}$$

which is to be solved subject to the boundary and interface conditions,

$$D\tilde{\theta}_1(-\delta) = 0, \quad \tilde{\theta}_1(0) = \tilde{\theta}_2(0), \quad \text{and} \quad dD\tilde{\theta}_1(0) = D\tilde{\theta}_2(0). \tag{B.2}$$

Eq. (B.1) has the general solution, $\tilde{\theta}_1 = A\cosh ky + B\sinh ky$, and when the above boundary condition at $y = -\delta$ is applied, then the following relation between A and B is obtained:

$$B\cosh k\delta - A\sinh k\delta = 0. \tag{B.3}$$

On applying the interface conditions at $y = 0$, we get the following expressions for $\tilde{\theta}_2(0)$ and $D\tilde{\theta}_2(0)$,

$$\tilde{\theta}_2(0) = A \quad \text{and} \quad D\tilde{\theta}_2(0) = dkB. \tag{B.4}$$

When these are substituted in Eq. (B.3), the following boundary condition may be derived,

$$D\tilde{\theta}_2(0) = kd(\tanh k\delta)\tilde{\theta}_2(0). \tag{B.5}$$

The equivalent condition for the upper boundary of the porous layer is,

$$D\tilde{\theta}_2(1) = -kd(\tanh k\delta)\tilde{\theta}_2(1). \tag{B.6}$$

While these boundary conditions may be interpreted quite correctly as being of mixed type, they nevertheless depend on the wavenumber, k. Therefore the presence of bounding plates cannot be modelled by a fixed Biot number, such as is used in [14]. The presence of k in Eqs. (B.5) and (B.6) implies that the results of the present cannot be inferred at least quantitatively from the analysis contained in [14].

Finally, it is important to note that (B.5) and (B.6) apply only when the onset of convection is stationary. Although the present problem does have stationary onset, the analogous layer with two diffusing components might be subject to overstability, and a more complicated pair of boundary conditions would then need to be derived.

References

[1] D.A. Nield, A. Bejan, Convection in Porous Media, Springer-Verlag, New York, 1998.
[2] D.B. Ingham, I. Pop, Transport Phenomena in Porous Media, vol. III, Pergamon Press, 2005.
[3] K. Vafai, Handbook of Porous Media, vol. 2, Marcel Dekker, New York/Basel, 2005. pp. 269–320.
[4] P. Vadász, in: Peter Vadász (Ed.), Theory and Applications of Transport in Porous Media, vol. 22, Springer, 2008, Hardcover, ISBN: 978-1-4020-8177-4.
[5] C.W. Horton, F.T. Rogers, Convection currents in porous media, J. Appl. Phys. 6 (1945) 367–370.
[6] E.R. Lapwood, Convection of a fluid in a porous medium, Proc. Camb. Philos. Soc. 44 (1948) 508–521.
[7] M.A. Combarnous, S.A. Bories, Hydrothermal convection in saturated porous media, Adv. Hydrosci. 10 (1975) 231.
[8] J.L. Beck, Convection in a box of porous material saturated with fluid, Phys. Fluids 15 (1972) 1377–1383.
[9] Y. Katto, T. Masuoka, Criterion for the onset of convective flow in a fluid in a porous medium, Int. J. Heat Mass Transfer 10 (1967) 297–409.
[10] R.J. Ribando, K.E. Torrance, Natural convection in a porous medium: effects of confinement, variable permeability, and thermal boundary conditions, J. Heat Transfer 98 (1976) 42.
[11] C.Y. Wang, Onset of convection in a fluid-saturated rectangular box, bottom heated by constant flux, Phys. Fluids 11 (6) (1999) 1675.
[12] P.K. Tewari, K.E. Torrance, Onset of convection in a box of fluid saturated porous material with a permeable top, Phys. Fluids 24 (1981) 981.
[13] D.S. Riley, K.H. Winters, Modal exchange mechanisms in Lapwood convection, J. Fluid Mech. 204 (1989) 325.
[14] J.P. Kubitschek, P.D. Weidman, Stability of a fluid-saturated porous medium contained in vertical cylinder heated from below by forced convection, Heat Mass Transfer 42 (2006) 789–794.
[15] D.A.S. Rees, P.A. Tyvand, Onset of convection in a porous layer with continuous periodic horizontal stratification. Part I. Two-dimensional convection, Transport Porous Med. 77 (2009) 187–205.
[16] D.A. Nield, A.V. Kuznetsov, The effects of combined horizontal and vertical heterogeneity and anisotropy on the onset of convection in a porous medium, Int. J. Therm. Sci. 46 (2007) 1211–1218.
[17] M. Mamou, P. Vasseur, Thermosolutal bifurcation phenomena in porous enclosures subject to vertical temperature and concentration gradients, J. Fluid Mech. 395 (1999) 61–87.
[18] M.C. Charrier-Mojtabi, B. Elhajjar, A. Mojtabi, Analytical and numerical stability analysis of Soret-driven convection in a horizontal porous layer, Phys. Fluids 19 (2007) 124104.
[19] I.G. Donaldson, Temperature gradients in the upper layers of the earth's crust due to convective water flows, J. Geophys. Res. 67 (1962) 3449–3459.
[20] J.Y. Jang, W.L. Tsai, Thermal instability of two horizontal porous layers with a conductive partition, Int. J. Heat Mass Transfer 31 (1988) 993–1003.
[21] D.N. Riahi, Nonlinear convection in a porous layer with finite conducting boundaries, J. Fluid Mech. 129 (1983) 153–171.
[22] B. Elhajjar, M.C. Charrier-Mojtabi, A. Mojtabi, Separation of a binary fluid mixture in a porous horizontal cavity, Phys. Rev. E 77 (2) (2008) 026310.
[23] R. Bennaceur, A. Mahidjiba, P. Vasseur, H. Beji, R. Duval, The Soret effect on convection in a horizontal porous domain under cross temperature and concentration gradients, Int. J. Numer. Methods Heat Fluid Flow 13 (2–3) (2003) 199–215.